CHEMICAL PHYSICS

Quantum control of molecular collisions at 1 kelvin

William E. Perreault, Nandini Mukherjee,* Richard N. Zare*

Measurement of vector correlations in molecular scattering is an indispensable tool for mapping out interaction potentials. In a coexpanded supersonic beam, we have studied the rotationally inelastic process wherein deuterium hydride (HD) (v = 1, j = 2) collides with molecular deuterium (D_2) to form HD (v = 1, j = 1), where v and j are the vibrational and rotational quantum numbers, respectively. HD (v = 1, j = 2) was prepared by Stark-induced adiabatic Raman passage, with its bond axis aligned preferentially parallel or perpendicular to the lab-fixed relative velocity. The coexpansion brought the collision temperature down to 1 kelvin, restricting scattering to s and p partial waves. Scattering angular distributions showed a dramatic stereodynamic preference (~3:1) for perpendicular versus parallel alignment. The four-vector correlation measured between the initial and final velocities and the initial and final rotational angular momentum vectors of HD provides insight into the strong anisotropic forces present in the collision process.

One of the most fundamental goals in chemical physics is to understand the interaction forces that bind matter together at the quantum level. Scattering experiments have proven to be a powerful tool for probing these inherently anisotropic forces (*1*, *2*). The field of cold collision dynamics (temperatures of 1 to 2 K) was born out of the recognition that, at ambient temperatures, information about the interaction potential is blurred by the presence of many orbital angular momentum states (partial waves) associated with the translational degrees of freedom of a scattering interaction (*3*, *4*). To gain a clear understanding of the interaction potential, it is therefore essential to reduce the energy at which the collision occurs, as this removes partial waves of higher angular momentum. One commonly used technique to reach temperatures of a few kelvin is paired molecular beams (*5*, *6*) using a variety of techniques, including decelerating to low velocities (*7*), crossing at shallow angles (*8*), and merging (*9*–*11*). Here we use a technologically simpler method of generating collisions, whereby both partners in the colliding pair are supersonically expanded in the same jet, which brings the collision temperature down near 1 K. This technique bears some similarity to the well-established CRESU technique, although CRESU has never reached collision temperatures below 8 K (*12*). At temperatures near 1 K, the de Broglie wavelength becomes comparable in dimension to the long-range portion of the interaction potential, which is extremely sensitive to the anisotropy resulting from molecular orientation (*4*, *13*). This imposes a second important condition: The initial internal quantum state of the molecules must be completely defined. Otherwise, averaging over a large number of states will wash out signatures of the anisotropic part of the interaction potential.

Over the years, many methods have been developed to prepare or select both specific internal energy states and molecular orientation and alignment for use in collision experiments (*14*–*16*). These include brute force orientation (*17*), hexapole state selection (*18*–*20*), and optical pumping (*21*–*23*). Until recently, however, it remained difficult to prepare sufficient concentrations of specific quantum states of H_2 to obtain a reasonable signal-to-noise ratio in a scattering experiment. H_2 is particularly important because it is both the most abundant neutral molecule in the universe and the most tractable theoretically. Stark-induced adiabatic Raman passage (SARP) can prepare specific rovibrationally excited, aligned states of H_2 and its isotopologues (*24*, *25*). By selecting specific m states (m gives the projection of the rotational angular momentum vector on a quantization axis) within a single rovibrational (v, j) energy eigenstate, where v and j are the vibrational and rotational quantum numbers, respectively, SARP polarizes the angular momentum vector **j**, thus allowing full stereodynamic control of a scattering experiment. Although stereodynamic control has been demonstrated in ultracold polar molecules oriented by using electric fields (*26*), SARP allows both control of nonpolar homonuclear diatomic molecules at a wide range of temperatures and observation of collisions under field-free conditions.

Quantum state preparation using SARP combined with coexpansion of the colliding partners in a single beam provides a simple experimental method to simultaneously define both the internal and external (orbital angular momentum) quantum states for collisions involving hydrogen molecules. By selecting specific m states, SARP defines the direction of the angular momentum vector, or the axis of the molecular gyroscope, relative to the direction of approach. Performing collision experiments with hydrogen molecules prepared in this way allows the characterization of fundamental potential energy surfaces by directly relating experimental results to theoretical predictions without averaging. Experiments of this sort are essential to understand the quantum mechanics of molecular interactions.

A large number of theoretical studies on inelastic collisions involving hydrogen molecules have been done in the past, which systematically point to the presence of resonances near 1 K (*27*–*30*). These resonances suggest that strong van der Waals forces may govern these collisions, but no experiments have yet tested any of these predictions. Previous H_2 scattering experiments have been conducted at collision energies considerably higher than the energy separation of the rotational states (*31*–*33*). At these high collision energies, analysis of the experimental data, which necessarily involves a large number of partial waves, has yielded useful, but limited, information about the interaction potential.

We describe a low-energy scattering experiment of HD with D_2 coexpanded in a single supersonic beam with a 1:5.5 ratio of HD to D_2. SARP was used to prepare HD in specific m states of a rovibrationally excited (v = 1, j = 2) energy eigenstate. By preparing HD, we are able to take advantage of the strong Δj = 1 rotational relaxation HD (v = 1, j = 2)→HD (v = 1, j = 1). A detailed description of the state preparation as well as the scattering experiment is given in the supplementary materials and methods. By selecting specific m quantum states and limiting the partial wave components to s (l = 0) and p (l = 1), where l is the orbital angular momentum quantum number, we measure a four-vector correlation, namely **k**-**j**-**k′**-**j′**, where **k** and **k′** are the initial and final velocity vectors of HD in the center-of-mass frame, and **j** and **j′** are the initial and final rotational angular momentum vectors of HD. The importance of vector correlations for understanding stereodynamics in molecular collisions has been recognized since the pioneering work of Herschbach and co-workers (*34*–*36*).

Figure 1A shows the speed distributions of HD and D_2 in the coexpanded molecular beam, which were calculated from time-of-flight measurements of HD (v = 1, j = 2) and D_2 (v = 0, j = 0) after (2 + 1) resonance enhanced multiphoton ionization (REMPI). There is a small, but finite, slip (~46 m/s) in their speed distribution. The collision temperature is ~1 K, as determined from the mean relative speed distribution shown in Fig. 1B. Measurement of the rotational distribution shows that in the molecular beam, 59% of the D_2 molecules are found in (v = 0, j = 0), 33% in (v = 0, j = 1), and 8% in (v = 0, j = 2). D_2 molecules were used without further state preparation. Greater than 98% of the HD molecules are in the ground state (v = 0, j = 0), which allows SARP to prepare nearly the entire HD population in a single rovibrationally excited state.

As detailed in the supplementary materials and methods, HD molecules were prepared in the (v = 1, j = 2, m = 0) state using SARP with a delayed sequence of a single-mode pump pulse and a single-mode Stokes pulse transversely

Department of Chemistry, Stanford University, Stanford, CA 94305, USA.
*Corresponding author. Email: zare@stanford.edu (R.N.Z.); nmukherj@stanford.edu (N.M.)

intersecting the molecular beam within the high-vacuum reaction chamber. As has been demonstrated in earlier work, by using partially overlapping pump and Stokes pulses, we achieved near complete population transfer from HD ($v = 0, j = 0$) to HD ($v = 1, j = 2, m = 0$). More detailed information on the SARP process can be found elsewhere (*24*, *37*).

Figure 2 shows the parallel and perpendicular collision geometries, indicated by H-SARP and V-SARP, respectively. In H-SARP (Fig. 2A), we align the HD ($v = 1, j = 2$) molecular bond axis preferentially parallel to the flight direction using linearly polarized pump and Stokes pulses with their direction of polarization aligned along the molecular beam axis. In V-SARP (Fig. 2B), we align the HD ($v = 1, j = 2$) molecular bond axis preferentially perpendicular to the flight direction using pump and Stokes pulses perpendicularly polarized with respect to the molecular beam axis. Because the colliding partners HD and D_2 are coexpanded in a single molecular beam, the direction of their relative velocity is extremely well defined (±10 mrad). By aligning the molecular bond axis parallel (H-SARP) and perpendicular (V-SARP) to the relative velocity of the colliding partners, we are able to achieve a high degree of stereodynamic control over the scattering interaction.

Figure 3 shows the time-of-flight distribution of the scattered HD ($v = 1, j = 1$) for both H-SARP and V-SARP. Within experimental uncertainty, the same distributions are recorded for a 1:29 HD:D_2 mixture, showing that collisions of HD with itself make no notable contribution to the observed time-of-flight spectrum. The experimental data in Fig. 3 demonstrates remarkable stereodynamic effects, with V-SARP nearly three times as strong as H-SARP, in the total and differential scattering cross sections. The energy released by the rotational relaxation of HD ($v = 1, j = 2$)→HD ($v = 1, j = 1$) is insufficient to rotationally excite D_2 because electrostatic interactions are unlikely to change nuclear spin, precluding ortho-to-para conversion. Fitting the time-of-flight distribution of the unscattered HD ($v = 1, j = 2$) molecules, given by the magenta curves in Fig. 3, allows us to extract the mean molecular beam velocity. Because the center-of-mass frame coincides with the lab frame moving at the mean velocity of the unscattered HD molecules, the conversion from time-of-flight to scattering angle is simplified, as detailed in the supplementary text.

We have performed a partial-wave analysis of the time-of-flight distribution shown in Fig. 3, A and B. For the analysis, we assumed the quantization z axis oriented along the relative velocity of the colliding partners, which coincides with the lab-frame molecular beam axis as well as the time-of-flight axis. The relation between the center-of-mass scattering angle (θ) and the measured time-of-flight is detailed in the supplementary text. The angular distribution, $d\sigma/d\theta$, of inelastically scattered HD ($v = 1, j = 1$) as a function of the polar angle (θ) is obtained by integrating the differential scattering cross section, $d\sigma/d\Omega$, per unit solid angle over all azimuthal angles (φ)

$$\frac{d\sigma}{d\theta}(j=2\rightarrow j=1)=\sin\theta\int_0^{2\pi}\left[\left(\frac{d\sigma}{d\Omega}\right)_{j=1,m_f=0}+\left(\frac{d\sigma}{d\Omega}\right)_{j=1,m_f=+1}+\left(\frac{d\sigma}{d\Omega}\right)_{j=1,m_f=-1}\right]d\varphi \quad (1)$$

where $d\Omega$ gives the differential solid angle in the direction defined by θ and φ. For clarity, m_f refers to the z-axis projection of the angular momentum vector **j** of the scattered HD ($v = 1, j = 1$), whereas m refers to that of the unscattered HD ($v = 1, j = 2$). In Eq. 1, $\left(\frac{d\sigma}{d\Omega}\right)_{j=1,m_f}$ represents the differential scattering cross section for a given outgoing channel, with $j = 1$, $m_f = 0, \pm 1$. The partial-wave analysis described in the supplementary material is considerably simplified when the angular momentum quantization axis lies along the time-of-flight axis. In reference to this system of coordinate axes (see Fig. 2A), the state prepared using V-SARP becomes a

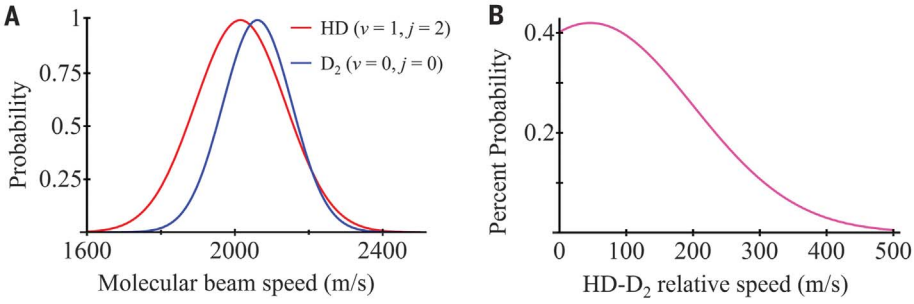

Fig. 1. Molecular beam speed distributions. (**A**) Gaussian fits of experimentally determined speed distributions of HD ($v = 1, j = 2$), given by $P_{HD}(u) = \exp\{-[(u - 2015)/173]^2\}$, and D_2 ($v = 0, j = 0$), given by $P_{D_2}(u) = \exp\{-[(u - 2061)/132]^2\}$, where u is the speed of the molecule along the time-of-flight axis. These speed distributions are derived from the time-of-flight data provided in data files S1 (D_2) and S2 (HD). (**B**) Relative speed distribution between HD ($v = 1, j = 2$) and D_2 ($v = 0, j = 0$) derived from the convolution of the two measured speed distributions shown in (A). This distribution gives a mean collision energy of ~1 K, corresponding to a mean relative speed of ~100 m/s.

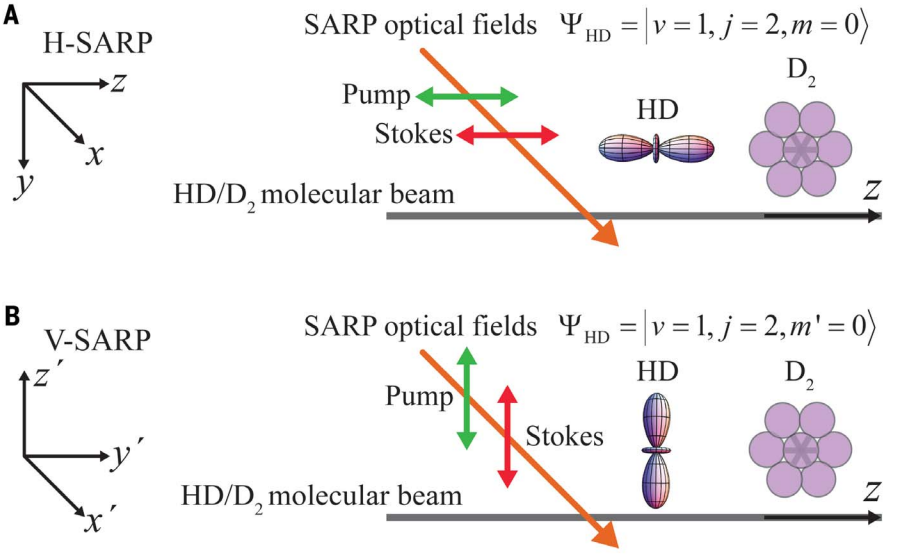

Fig. 2. Two different HD–D_2 collision geometries. The quantum state of HD is prepared by using SARP optical fields polarized (**A**) parallel (H-SARP) and (**B**) perpendicular (V-SARP) to the molecular beam axis. The green and red arrows represent the polarization directions of the optical fields associated with the pump and Stokes laser pulses, respectively. For H-SARP, the m state refers to the quantization z axis parallel to the relative velocity of HD and D_2. For V-SARP, the m' state refers to the quantization z' axis perpendicular to the relative velocity. For H-SARP, the HD molecular bond axis is preferentially aligned parallel to the relative velocity, and for V-SARP, the HD bond axis is preferentially aligned perpendicular to the relative velocity of HD and D_2. Because D_2 is not state prepared, its axis is distributed isotropically.

superposition of m = 0 and m = ±2 states as follows:

$$|j=2,m'=0\rangle = \sqrt{\frac{3}{8}}|j=2, m=+2\rangle - \frac{1}{2}|j=2,m=0\rangle + \sqrt{\frac{3}{8}}|j=2,m=-2\rangle \quad (2)$$

For simplicity, the vibrational quantum number (v = 1) is omitted in Eqs. 1 to 4. Each outgoing channel of the scattered HD (j = 1, m_f) will have contributions from all three input channels, HD (j = 2, m = 0, ±2), in Eq. 2. Therefore, for each outgoing channel (designated by a given value of m_f), the scattered angular distribution for V-SARP results from the interference of the scattering amplitudes associated with the three input channels as follows:

$$\left(\frac{d\sigma}{d\Omega}\right)^{V}_{j=1,m_f} = \left|\sqrt{\frac{3}{8}}q_{j=2,m=+2\to j=1,m_f} - \frac{1}{2}q_{j=2,m=0\to j=1,m_f} + \sqrt{\frac{3}{8}}q_{j=2,m=-2\to j=1,m_f}\right|^2 \quad (3)$$

In Eq. 3, $q_{j=2,m\to j=1,m_f}$ represents the state-to-state scattering amplitude within a differential solid angle dΩ along the direction (θ, ϕ) defined with respect to the quantization z axis. For H-SARP, where the direction of laser polarization is parallel to the quantization z axis (see Fig. 2A), no coordinate transform is needed, and the differential scattering cross section for an outgoing channel with a specific value of m_f is given by

$$\left(\frac{d\sigma}{d\Omega}\right)^{H}_{j=1,m_f} = \left|q_{j=2,m=0\to j=1,m_f}\right|^2 \quad (4)$$

On the basis of prior calculations on H_2–H_2 rotational relaxation (*38*), we assume a range of ~4 Å for the anisotropic part of the potential responsible for the Δj = 1 rotational relaxation in this HD–D_2 collision. At the collision energies of ~0.1 meV present in our experiment, this range limits the dominant contributing partial waves to s and p. Considering contributions of only the s and p partial waves in the input channel, we are able to derive an expression for the state-to-state scattering amplitude $q_{j=2,m\to j=1,m_f}$ as a sum of the outgoing partial waves described by the spherical harmonics Y_{lm}. Here, l and m refer to the outgoing orbital angular momentum and its projection on the quantization z axis. The details of this derivation are given in an exemplary case in the supplementary materials, along with the derived scattering angular distributions, which are obtained after replacing each state-to-state scattering amplitude $q_{j=2,m\to j=1,m_f}$ in Eqs. 3 and 4 in terms of the outgoing spherical waves. The derived scattering angular distributions derived in this way were used to fit the experimental data shown in Fig. 3. This fitting procedure enables the separation of the contributions of the outgoing channels with different values of m_f, which correspond to different angular momentum polarizations of the scattered HD (v = 1, j = 1).

Figure 4, A and B, show the fit-generated scattering angular distributions, $\left(\frac{d\sigma}{d\theta}\right)_{j=1,m_f}$, for different angular momentum polarizations m_f = 0, ±1 of the scattered HD (v = 1, j = 1), for the initial HD molecules prepared by H-SARP and V-SARP, respectively. The green and red curves (in Fig. 4, A and B, respectively), are generated by the same theoretical fits of the experimental data as the black curves shown in Fig. 3, A and B. These fits had coefficient of determination (R^2) values greater than 0.99. There is a clear correlation between the peaks in the time-of-flight distribution of Fig. 3 and the components (m_f = 0, ±1) of the angular momentum vector of the outgoing scattered HD (v = 1, j = 1). Partial-wave analysis allows us to determine the direction of the final angular momentum **j′** as a function of the scattering angle **k′**. Because the initial velocity **k** is well defined by the molecular beam axis and the direction of the initial angular momentum vector **j** is controlled by SARP, we are able to measure the four-vector correlation, **k-j-k′-j′**.

From the derived polarization-dependent angular distribution, it is immediately apparent that the angular momentum polarization present in the initial HD molecules has been lost. For both

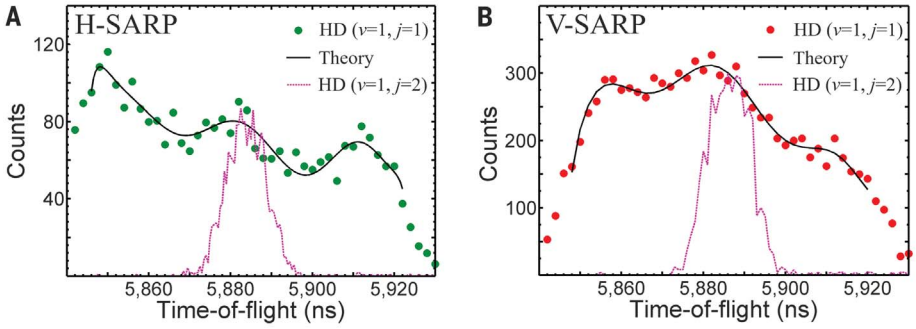

Fig. 3. Time-of-flight distribution of rotationally relaxed HD (v = 1, j = 1). Collisions of state-prepared HD (v = 1, j = 2) with unprepared D_2 occurred in a supersonically coexpanded beam of a 1:5.5 HD:D_2 mixture, where the HD molecular bond axis was aligned (**A**) parallel (H-SARP) or (**B**) perpendicular (V-SARP) to the relative velocity between HD and D_2. The magenta dashed curve gives the time-of-flight distribution of unscattered state-prepared HD (v = 1, j = 2), which has been scaled to match the scattered distribution height and therefore serves only as a visual reference of the initial velocity distribution. In both (A) and (B), the black solid curve (theory) shows fitting using partial wave analysis as described in the text. The time-of-flight data plotted in (A) and (B) can be found in data files S3 and S5, respectively. Both data files have been background subtracted to remove off-resonantly generated ions. The H-SARP data (data file S3) shown in (A) has been normalized to the REMPI power and the total experimental run time used in the collection of the V-SARP data (data file S5) shown in (B). The time-of-flight data for the unscattered HD (v = 1, j = 2) can be found in data files S4 (H-SARP) and S6 (V-SARP). Counts, the total number of scattered HD (v = 1, j = 1) molecules detected in a given time-of-flight interval over the duration of the scattering experiment.

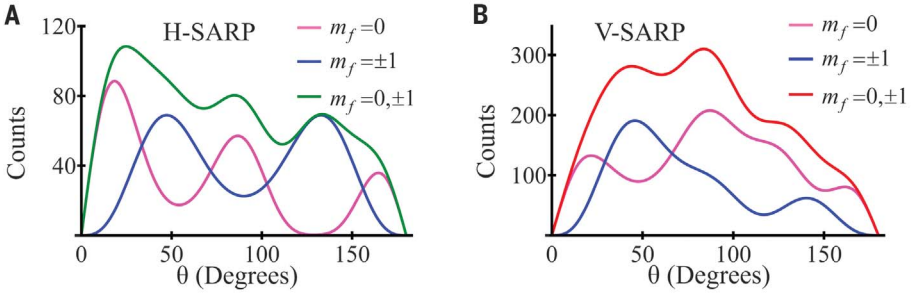

Fig. 4. Angular distribution of scattered HD (v = 1, j = 1) showing m_f-state dependence. Each curve gives $\left(\frac{d\sigma}{d\Omega}\right)_{j=1,m_f}$ for the indicated value of m_f. (**A**) HD bond axis preferentially aligned along the molecular beam axis (H-SARP). (**B**) HD bond axis preferentially polarized perpendicular to the molecular beam axis (V-SARP). m_f refers to the angular momentum component of the scattered HD (v = 1, j = 1) relative to the quantization z axis parallel to the molecular beam axis. The curves labeled m_f = 0, ±1 in each plot give the theoretical scattering distribution, $\sum_{m_f=-1}^{+1}\left(\frac{d\sigma}{d\theta}\right)_{j=1,m_f}$, obtained by fitting the experimental data presented in Fig. 3. The angular distributions for specific outgoing angular momentum polarization are given by the blue and magenta curves.

H-SARP and V-SARP prepared HD, the scattered molecules have not preserved the initial molecular alignment. Although this behavior contradicts the well-known $\Delta m = 0$ selection rule for collisions (*39*–*41*), this is to be expected for molecular scattering where the depth of the anisotropic potential is substantially greater than the collision energy. As such, the observed depolarization provides clear evidence of anisotropic interactions that strongly couple the internal and orbital angular momenta. These strong forces suggest that a transient van der Waals complex may be present at the collision energies of this experiment.

We can make an order-of-magnitude estimate of the total collision cross section using a procedure that is described in the supplementary materials. For the initial HD molecular state prepared by V-SARP, we find an integral cross section of ~42 Å^2, whereas for the state prepared by H-SARP, it is reduced by a factor of 3 to ~14 Å^2. Our estimated cross section seems to agree with a prior theoretical prediction (*30*) within an order of magnitude, suggesting again the presence of a van der Waals resonance as described in that reference.

Without both HD state preparation using SARP and reduction in the number of involved partial waves due to the cold collisions present in the coexpanded molecular beam of mixed gases, the remarkable stereodynamic information revealed in these experiments would have been obscured. This study demonstrates conclusively the importance for collision dynamics of the preparation of initial quantum state of the entire system, including all possible degrees of freedom.

REFERENCES AND NOTES

1. D. Herschbach, *Faraday Discuss.* **142**, 9–23 (2009).
2. R. N. Zare, *Science* **279**, 1875–1879 (1998).
3. R. V. Krems, *Phys. Chem. Chem. Phys.* **10**, 4079–4092 (2008).
4. P. F. Weck, N. Balakrishnan, *Int. Rev. Phys. Chem.* **25**, 283–311 (2006).
5. C. Naulin, M. Costes, *Int. Rev. Phys. Chem.* **33**, 427–446 (2014).
6. J. Jankunas, A. Osterwalder, *Annu. Rev. Phys. Chem.* **66**, 241–262 (2015).
7. J. J. Gilijamse, S. Hoekstra, S. Y. T. van de Meerakker, G. C. Groenenboom, G. Meijer, *Science* **313**, 1617–1620 (2006).
8. S. Chefdeville *et al.*, *Science* **341**, 1094–1096 (2013).
9. A. B. Henson, S. Gersten, Y. Shagam, J. Narevicius, E. Narevicius, *Science* **338**, 234–238 (2012).
10. A. Klein *et al.*, *Nat. Phys.* **13**, 35–38 (2017).
11. J. Jankunas, B. Bertsche, K. Jachymski, M. Hapka, A. Osterwalder, *J. Chem. Phys.* **140**, 244302 (2014).
12. B. R. Rowe, J. B. Marquette, *Int. J. Mass Spectrom. Ion Process.* **80**, 239–254 (1987).
13. Y. Shagam *et al.*, *Nat. Chem.* **7**, 921–926 (2015).
14. H. J. Loesch, *Annu. Rev. Phys. Chem.* **46**, 555–594 (1995).
15. M. Brouard, D. H. Parker, S. Y. T. van de Meerakker, *Chem. Soc. Rev.* **43**, 7279–7294 (2014).
16. F. J. Aoiz *et al.*, *Phys. Chem. Chem. Phys.* **17**, 30210–30228 (2015).
17. H. J. Loesch, A. Remscheid, *J. Chem. Phys.* **93**, 4779–4790 (1990).
18. E. M. Jones, P. R. Brooks, *J. Chem. Phys.* **53**, 55–58 (1970).
19. J. J. van Leuken, F. H. W. van Amerom, J. Bulthuis, J. G. Snijders, S. Stolte, *J. Phys. Chem.* **99**, 15573–15579 (1995).
20. M. Brouard *et al.*, *J. Chem. Phys.* **141**, 164306 (2014).
21. E. A. Rohlfing, D. W. Chandler, D. H. Parker, *J. Chem. Phys.* **87**, 5229–5237 (1987).
22. P. Dittmann *et al.*, *J. Chem. Phys.* **97**, 9472–9475 (1992).
23. K. Liu, *J. Chem. Phys.* **142**, 080901 (2015).
24. W. Dong, N. Mukherjee, R. N. Zare, *J. Chem. Phys.* **139**, 074204 (2013).
25. N. Mukherjee, W. Dong, R. N. Zare, *J. Chem. Phys.* **140**, 074201 (2014).
26. M. H. G. de Miranda *et al.*, *Nat. Phys.* **7**, 502–507 (2011).
27. N. Balakrishnan, R. C. Forrey, A. Dalgarno, *Phys. Rev. Lett.* **80**, 3224–3227 (1998).
28. N. Uudus, S. Magaki, N. Balakrishnan, *J. Chem. Phys.* **122**, 024304 (2005).
29. T.-G. Lee *et al.*, *J. Chem. Phys.* **125**, 114302 (2006).
30. R. A. Sultanov, D. Guster, S. K. Adhikari, *J. Phys. At. Mol. Opt. Phys.* **49**, 015203 (2016).
31. U. Buck, F. Huisken, J. Schleusener, *J. Chem. Phys.* **68**, 5654–5655 (1978).
32. U. Buck, F. Huisken, J. Schleusener, J. Schäfer, *J. Chem. Phys.* **72**, 1512–1523 (1980).
33. J. Arnold, T. Dreier, D. W. Chandler, *Chem. Phys.* **133**, 123–136 (1989).
34. J. D. Barnwell, J. G. Loeser, D. R. Herschbach, *J. Phys. Chem.* **87**, 2781–2786 (1983).
35. G. M. McClelland, D. R. Herschbach, *J. Phys. Chem.* **83**, 1445–1454 (1979).
36. D. A. Case, D. R. Herschbach, *Mol. Phys.* **100**, 109–125 (2002).
37. W. E. Perreault, N. Mukherjee, R. N. Zare, *J. Chem. Phys.* **145**, 154203 (2016).
38. U. Buck, *Faraday Discuss. Chem. Soc.* **73**, 187–203 (1982).
39. D. W. Chandler, R. L. Farrow, *J. Chem. Phys.* **85**, 810–816 (1986).
40. G. O. Sitz, R. L. Farrow, *J. Chem. Phys.* **101**, 4682–4687 (1994).
41. A. J. McCaffery, M. J. Proctor, B. J. Whitaker, *Annu. Rev. Phys. Chem.* **37**, 223–244 (1986).

ACKNOWLEDGMENTS

This work has been supported by the U.S. Army Research Office under Army Research Office (ARO) grant no. W911NF-16-1-1061 and Multidisciplinary University Research Initiatives (MURI) grant no. W911NF-12-1-0476. Data are available in the supplementary materials.

SUPPLEMENTARY MATERIALS

www.sciencemag.org/content/358/6361/356/suppl/DC1
Materials and Methods
Supplementary Text
Fig. S1
Reference (*42*)
Data Files S1 to S6

6 July 2017; accepted 8 September 2017
10.1126/science.aao3116

Quantum control of molecular collisions at 1 kelvin

William E. Perreault, Nandini Mukherjee and Richard N. Zare

Science **358** (6361), 356-359.
DOI: 10.1126/science.aao3116

Tracking collisions in just one beam

Much of what we know about how quantum mechanics dictates chemical dynamics comes from half a century of studying controlled collisions between crossed pairs of molecular beams. Perreault *et al.* now show that even finer detail emerges in a study of hydrogen-deuterium (HD) collisions with D_2 in a single beam. The experimental setup lowers the collision temperature to ~1 K, allowing precise control over the rotational energy and relative alignment of the colliding partners. Scattering events in which HD loses rotational energy occurred three times as readily if the HD was aligned perpendicular rather than parallel to the beam-propagation axis.

Science, this issue p. 356